



Contents lists available at ScienceDirect

Econometrics and Statistics

journal homepage: www.elsevier.com/locate/ecosta



Modeling Turning Points in the Global Equity Market

Daniel Felix Ahelegbey^a, Monica Billio^b, Roberto Casarin^{b,*}

^a Department of Economics and Management, University of Pavia, Italy

^b Department of Economics, Ca' Foscari University of Venice, Italy



ARTICLE INFO

Article history:

Received 9 November 2020

Revised 8 October 2021

Accepted 8 October 2021

Available online 27 October 2021

JEL classification:

C11

C15

C51

C52

C55

C58

G01

Keywords:

Bayesian inference

Dynamic Programming

Turning points

Networks

VAR

ABSTRACT

Turning points in financial markets are often characterized by changes in the direction and/or magnitude of market movements with short-to-long term impacts on investors' decisions. A Bayesian technique is developed for turning point detection in financial equity markets. The interconnectedness among stock market returns from a piece-wise network vector autoregressive model is derived. The turning points in the global equity market over the past two decades are examined in the empirical application. The level of interconnectedness during the Covid-19 pandemic and the 2008 global financial crisis are compared. Similarities and most central markets responsible for spillover propagation emerged from the analysis.

© 2021 The Authors. Published by Elsevier B.V. on behalf of EcoSta Econometrics and Statistics.

This is an open access article under the CC BY license
(<http://creativecommons.org/licenses/by/4.0/>)

1. Introduction

The turn of events in major financial markets since late February 2020, following the spread of the novel Coronavirus from Wuhan, in China, to a global pandemic, is certainly a reminder of the increased interconnectedness of the global market. Connectedness plays a substantial role in the contagion spreading, especially during turbulent periods. Thus, a better understanding of the interconnectedness dynamics is critical to uncover potential contagion effects and support risk management decisions. Modeling interconnectedness has received much attention, especially after the 2007–2009 global financial crisis, and the 2010–2013 European sovereign debt crisis (see Ahelegbey et al., 2016a; Billio et al., 2012; Battiston et al., 2012; Diebold and Yilmaz, 2014; DasGupta and Kaligounder, 2014; Hautsch et al., 2015; Billio et al., 2019; Casarin et al., 2020).

In investigating interconnectedness dynamics, it has become necessary to account properly for structural changes. For instance, financial institutions are often interconnected through diverse channels, ranging from inter-bank market transfers, direct deposits, relationship lending/borrowing, and exposures to common risk or market factors. These connections are often characterized by sudden changes in direction and magnitude with short-to-long term impacts on investors' decisions.

* Corresponding author. Tel.: +390412349149.

E-mail addresses: danielfelix.ahelegbey@unipv.it (D.F. Ahelegbey), billio@unive.it (M. Billio), r.casarin@unive.it (R. Casarin).

Turning points may occur due to changes in policy regimes, fluctuations in underlying market conditions, or changes in the financial health of counterparties.

From a modeling perspective, structural changes can produce bias in risk measure estimation and large forecasting errors, as the use of old data becomes counter-productive (see Chib, 1998; Bai, 2000; Pesaran et al., 2006; Qu and Perron, 2007; Ruggieri, 2013; Cho and Frylewicz, 2015). This paper contributes to the above discussion by advancing a Bayesian technique to change point detection in financial time series. We formalize the interconnectedness among stock returns with a piece-wise vector autoregressive model (VAR) with residual structural equations (RSEM). Our model accounts for the contemporaneous, lagged, and cross-lagged dependencies beyond what simple stylized facts from historical data can provide. Moreover, in large VAR models, there are too many parameters to estimate compared to the available observations (e.g., see Hauzenberger, 2021; Ankargren and Jonéus, 2021; Hu et al., 2020). A natural approach to overcome over-parametrization is via variable selection to produce parsimonious and sparse models. Graphical modeling presents a convenient framework to achieve parsimony while providing explainable interactions in multivariate time series (Ahelegbey et al., 2016a). Closely related models have in recent times been applied to infer financial contagion networks (e.g., see Ahelegbey et al., 2016a; 2016b; Billio et al., 2012; Basu and Michailidis, 2015; Barigozzi and Brownlees, 2019; Diebold and Yilmaz, 2014; Billio et al., 2019; Bianchi et al., 2019) and macroeconomic spillover networks (e.g., see Agudze et al., 2021; Skripnikov and Michailidis, 2019).

Recent studies recognized the relevance of structural breaks in connectedness analysis and proposed new modeling and inference solutions for large panel of time series. For example Massacci (2017, 2021) proposed regime changes in large dimensional factor models through a threshold mechanism and considered connectedness measures based on covariance matrices. Bianchi et al. (2019) assumed a latent Markov switching process driving covariance restrictions in high-dimensional SUR models and studied connectedness based on network. The concept adopted in this paper places our contribution within the literature on change detection in multivariate time series and specifically to Bayesian turning point models (Koop and Potter, 2007; 2009; Jochmann et al., 2010), turning point network models (Barnett and Onnela, 2016; Xuan and Murphy, 2007; Lèbre et al., 2010; Grzegorczyk et al., 2011), high dimensional Bayesian models (Koop et al., 2019; Ahelegbey et al., 2016b; Gruber and West, 2017), and graphical models (see Ahelegbey et al., 2016a; 2016b; Corander and Villani, 2006; Paci and Consonni, 2020; Gruber and West, 2017). In this paper, we adopt a specification strongly connected to the Bayesian turning point model of Jochmann et al. (2010), the changing dependency structure of Xuan and Murphy (2007), and extension of the Bayesian graphical VAR (BGVAR) model of Ahelegbey et al. (2016a) to allow for structural changes.

Several techniques for estimating turning point locations have dominated the Bayesian literature. Prominent among such techniques are the ones based on Markov chain Monte Carlo (MCMC) (Barry and Hartigan, 1993; Green, 1995; Western and Kleykamp, 2004; Erdman and Emerson, 2008) and recursive dynamic programming algorithms (Fearnhead, 2006; Fearnhead and Liu, 2007; Ruggieri, 2013). However, turning point estimation in high-dimensional models presents several inferential and computational challenges. In such settings, standard MCMC-based techniques usually suffer from slow mixing and high computational cost. We, therefore, propose a sequential turning point detection algorithm for BGVAR. The algorithm is an extension to multiple-equation models of the dynamic programming approach given in Ruggieri and Antonellis (2016) for single-equation models. This approach proves to be very effective in inferring the number and the timing of the turning points, reducing the computational cost for large data sets.

We apply our proposed model to the global equity market by considering the 15 major stock markets, including the G10 countries. The dataset consists of daily prices from Bloomberg, covering January 28, 1999, to April 30, 2021. The empirical application examines the turning points, compares the connectedness level during the Covid-19 and global financial crisis periods, and identifies the most relevant markets in the spillover propagation.

The paper is organized as follows. Section 2 presents the piece-wise BGVAR model and discusses the inference procedure. Section 3 presents a description of the data and reports the results in Section 4. Section 5 concludes the paper.

2. A Bayesian Graphical Piece-Wise Vector Autoregression

2.1. Piece-Wise VAR Model

Let $Y_t = (Y_{1,t}, \dots, Y_{n,t})$ be an n -variable vector of observed returns at time t , with $t = 1, \dots, T$, where $Y_{i,t}$ is the time series of market i at time t . Suppose there exist k turning points at $1 = \tau_0 < \tau_1 < \tau_2 < \dots < \tau_k < \tau_{k+1} = T$. We represent the dynamics of Y_t as piece-wise stationary vector autoregressive (VAR) model of order p given by

$$Y_t = \sum_{s=1}^p B_s^{(l)} Y_{t-s} + U_t^{(l)}, \quad t \in (\tau_{l-1}, \tau_l], \quad (1)$$

$$U_t^{(l)} = B_0^{(l)} U_t^{(l)} + \varepsilon_t^{(l)}, \quad \varepsilon_t^{(l)} \sim \mathcal{N}(0, \Sigma_\varepsilon^{(l)}), \quad (2)$$

where p is the lag order, $B_s^{(l)}$ is an $n \times n$ matrix of coefficients with $B_{ij,s}^{(l)}$ measuring the effect of $Y_{j,t-s}$ on $Y_{i,t}$ for $t \in (\tau_{l-1}, \tau_l]$, $l = 1, \dots, k+1$, $B_0^{(l)}$ is a full (non-symmetric) matrix with zeroes on the main diagonal that records the contemporaneous effect of shocks, $U_t^{(l)}$ is a vector independent and identically normal residuals with covariance matrix $\Sigma_u^{(l)}$, and $\varepsilon_t^{(l)}$ is a

vector of idiosyncratic components of the structural (and mutually orthogonal) shocks with diagonal covariance matrix $\Sigma_{\varepsilon}^{(l)}$. From Eq. (2), the $\Sigma_u^{(l)}$ can be expressed in terms of $B_0^{(l)}$ and $\Sigma_{\varepsilon}^{(l)}$ as

$$\Sigma_u^{(l)} = (I - B_0^{(l)})^{-1} \Sigma_{\varepsilon}^{(l)} (I - B_0^{(l)})^{-1'}. \quad (3)$$

2.2. Network Models

Following Ahelegbey et al. (2016a), Eq. (1) can be operationalized as a network model, where the variables in Y_t are defined by nodes joined by a set of links, describing the statistical relationships between pairs of variables. The introduction of networks in VAR models helps to interpret the serial, temporal and contemporaneous relationships in a multivariate time series. To analyze Eqs. (1) and (2) through networks, we assign to each coefficient $B_{ij,s}^{(l)}$ in $B_s^{(l)}$ a corresponding latent indicator $G_{ij,s}^{(l)}$ in $G_s^{(l)} \in \{0, 1\}^{n \times n}$, such that for $i, j = 1, \dots, n$, and $s = 0, 1, \dots, p$:

$$B_{ij,s}^{(l)} = \begin{cases} 0 & \text{if } G_{ij,s}^{(l)} = 0 \Rightarrow Y_{j,t-s} \not\rightarrow Y_{i,t} \\ \beta_{ij,s}^{(l)} \in \mathbb{R} & \text{if } G_{ij,s}^{(l)} = 1 \Rightarrow Y_{j,t-s} \rightarrow Y_{i,t} \end{cases} \quad (4)$$

for $l = 1, \dots, k+1$, where $Y_{j,t-s} \not\rightarrow Y_{i,t}$ means that Y_j does not influence Y_i at lag s . When $s = 0$, $Y_{j,t} \not\rightarrow Y_{i,t}$ corresponds to contemporaneous independence.

Let $\tilde{B}_{ij}^{(l)} = \sum_{s=0}^p B_{ij,s}^{(l)}$ and $\tilde{G}_{ij}^{(l)} = \sum_{s=0}^p G_{ij,s}^{(l)}$. Following Eq. (4), we define two null-diagonal matrices $A^{(l)} \in \{0, 1\}^{n \times n}$ and $W \in \mathbb{R}^{n \times n}$, whose ij -th element is given by:

$$A_{ij}^{(l)} = \begin{cases} 0, & \text{if } \tilde{G}_{ij}^{(l)} = 0 \\ 1, & \text{otherwise} \end{cases}, \quad W_{ij}^{(l)} = \begin{cases} 0, & \text{if } \tilde{B}_{ij}^{(l)} = 0 \\ \tilde{B}_{ij}^{(l)}, & \text{otherwise} \end{cases}, \quad (5)$$

where $A_{ij}^{(l)}$ specifies that $Y_j \rightarrow Y_i$ exist if there is a contemporaneous or lagged directed link from Y_j to Y_i . $W_{ij}^{(l)}$ specifies the weights of such a relationship obtained as a sum of the estimated contemporaneous and lagged coefficients. The correspondence between $(G^{(l)}, B^{(l)})$ and $(A^{(l)}, W^{(l)})$ is such that the former captures the short-run dynamics in Y_t while the latter can be viewed as long-term direct relationships when $Y_t = Y_{t-1} = \dots = Y_{t-p}$. Defining a sparse structure on $(G^{(l)}, B^{(l)})$ induces parsimony of the short-run model and sparsity on the long-run relationship matrices $(A^{(l)}, W^{(l)})$, $l = 1, \dots, k+1$.

2.3. Bayesian Estimation of a Piece-Wise Network VAR

Following standard practice, we select the appropriate lag order of the VAR via a Bayesian information criterion (BIC). Thus, the parameters left to estimate in a piecewise network VAR are $(k, V_{\tau,k}, G_{1:k}, B_{1:k}, \Sigma_{\varepsilon,1:k})$, where k is the number of turning points, $V_{\tau,k} = (\tau_1, \tau_2, \dots, \tau_k)$ is the turning point locations, $G_{1:k} = \{G^{(1)}, \dots, G^{(k+1)}\}$ where $G^{(l)} = \{G_0^{(l)}, \dots, G_p^{(l)}\}$ is the collection of lag-specific graphs for the interval $(\tau_{l-1}, \tau_l]$, $B_{1:k} = \{B^{(1)}, \dots, B^{(k+1)}\}$ where $B^{(l)} = \{B_0^{(l)}, \dots, B_p^{(l)}\}$ is the collection of lag-specific coefficient matrices, and $\Sigma_{\varepsilon,1:k} = \{\Sigma_{\varepsilon}^{(1)}, \dots, \Sigma_{\varepsilon}^{(k+1)}\}$ is the collection of error covariance matrices over segments. Estimating these parameters jointly is a challenging problem and a computationally intensive exercise. We complete the Bayesian formulation with prior specification and posterior approximations to draw inference on the model parameters.

We specify the prior distributions over $(k, V_{\tau,k}, G_{1:k}, B_{1:k}, \Sigma_{\varepsilon,1:k})$ as follows:

$$\begin{aligned} k &\sim \mathcal{U}(0, k_{\max}), & V_{\tau,k} &\sim \mathcal{U}(1, T), & [B_{ij,s}^{(l)} | G_{ij,s}^{(l)} = 1] &\sim \mathcal{N}(0, \eta), \\ G_{ij,s}^{(l)} &\sim \text{Ber}(q_{ij}), & \Sigma_{\varepsilon}^{(l)-1} &\sim \mathcal{W}_G(\delta_{\varepsilon}, \Lambda_{\varepsilon,0}), & \Sigma_u^{(l)-1} &\sim \mathcal{W}(\delta_u, \Lambda_{u,0}) \end{aligned}$$

for $l = 1, \dots, k+1$, where k_{\max} , η , q_{ij} , δ_{ε} , δ_u , $\Lambda_{\varepsilon,0}$, and $\Lambda_{u,0}$ are hyper-parameters.

The specification for k is a discrete uniform prior on the set $\mathcal{K} = \{0, \dots, k_{\max}\}$, with density

$$P(k) = \frac{1}{k_{\max} + 1} \mathbf{1}_{\{k \in \mathcal{K}\}}. \quad (6)$$

The choice of the discrete uniform prior is relatively non-controversial since it is similar to the truncated Poisson in Nobile and Fearnside (2007); Grzegorczyk et al. (2011).

We consider τ_1, \dots, τ_k as order statistics and define $d_{\tau} = \tau_l - \tau_{l-1}$ as the distance between successive turning points. We consider $V_{\tau,k}$ to be uniformly distributed on $[1, T]$ with density

$$P(V_{\tau,k}|k) = \frac{1}{N_k}, \quad N_k \approx \binom{T_d}{k}, \quad (7)$$

where $T_d = T - d_{\tau}$, $\tau_0 = 1$ and $\tau_{k+1} = T$, N_k is a normalizing constant and $\binom{a}{b}$ denotes a binomial coefficient indexed by a and b . The motivation for this prior choice is to discourage short segments and to favour a priori an equal spacing of the turning points. Also it shows that close observations are likely to belong to the same segment.

Table 1
Description of stock market indices of countries classified according to regions.

Region	No.	Country	Code	Description	Index
Americas	1	Brazil	BR	Brazil Bovespa	IBOV
	2	Canada	CA	Canada TSX Comp.	SPTSX
	3	United States	US	United States S&P 500	SPX
Asia-Pacific	4	Australia	AU	Australia ASX 200	AS51
	5	China	CN	China SSE Comp.	SHCOMP
	6	Hong Kong	HK	Hong Kong Hang Seng	HSI
	7	India	IN	India BSE Sensex	SENSEX
	8	Japan	JP	Japan Nikkei 225	NKY
	9	Korea	KR	South Korean KOSPI	KOSPI
	10	France	FR	France CAC 40	CAC
	11	Germany	DE	Germany DAX 30	DAX
	12	Italy	IT	Italy FTSE MIB	FTSEMB
Europe	13	Russia	RU	Russia MOEX	IMOEX
	14	Spain	ES	Spain IBEX 35	IBEX
	15	United Kingdom	UK	UK FTSE 100	UKX

The specification for $B_{ij,s}^{(l)}$ conditional on $G_{ij,s}^{(l)}$ follows a normal distribution with zero mean and variance η . Thus, relevant explanatory variables that predict a response variable must be associated with coefficients different from zero and the rest are restricted to zero. We consider $G_{ij,s}^{(l)}$ as Bernoulli distributed with q_{ij} as the prior probability.

We assume $\Sigma_{\varepsilon}^{(l)-1}$ is a G-Wishart distributed with prior expectation $\delta_{\varepsilon}^{-1}\Lambda_{\varepsilon,0}$ and $\delta_{\varepsilon} > n$ the degrees of freedom parameter. The G-Wishart distribution is the conjugate prior for the precision matrix over $P^+(G_{\varepsilon})$, i.e., the set of all symmetric, positive definite matrices with zeros in the off-diagonal elements that correspond to missing edges in G_{ε} , the graph associated with $\varepsilon_t^{(l)}$. Since by assumption, the elements of $\varepsilon_t^{(l)}$ are mutually independent, G_{ε} is the empty graph, which implies that $\Sigma_{\varepsilon}^{(l)-1}$ is a diagonal positive random matrix.

We assume $\Sigma_u^{(l)-1}$ is Wishart distributed with prior expectation $\delta_u^{-1}\Lambda_{u,0}$ and $\delta_u > n$ the degrees of freedom parameter.

Given the data, Y , the lag order p , and the prior distributions on the parameters, we apply a collapsed Gibbs and approximate the posterior distribution by sampling sequentially from the following conditional distributions:

1. $P(k, V_{\tau,k}|Y, p)$,
2. $P(G_{1:p}^{(l)}|Y, p, k, V_{\tau,k})$,
3. $P(G_0^{(l)}|Y, p, k, V_{\tau,k}, G_{1:p}^{(l)})$,
4. $P(B_{1:p}^{(l)}|Y, p, k, V_{\tau,k}, G_{1:p}^{(l)}, \Sigma_u^{(l)})$,
5. $P(B_0^{(l)}|Y, p, k, V_{\tau,k}, G_{1:p}^{(l)}, G_0^{(l)}, B_{1:p}^{(l)}, \Sigma_{\varepsilon}^{(l)}, \Sigma_u^{(l)})$,
6. $P(\Sigma_{\varepsilon}^{(l)}|Y, p, k, V_{\tau,k}, G_{1:p}^{(l)}, G_0^{(l)}, B_{1:p}^{(l)}, B_0^{(l)}, \Sigma_u^{(l)})$,
7. $P(\Sigma_u^{(l)}|Y, p, k, V_{\tau,k}, G_0^{(l)}, G_{1:p}^{(l)}, B_{1:p}^{(l)}, B_0^{(l)}, \Sigma_{\varepsilon}^{(l)})$.

We sample the number of turning points and their locations $\{k, V_{\tau,k}\}$ following the procedure in [Ruggieri and Antonellis \(2016\)](#) and use an efficient MCMC algorithm for sampling $\{G_0^{(l)}, G_{1:p}^{(l)}, B_0^{(l)}, B_{1:p}^{(l)}, \Sigma_{\varepsilon}^{(l)}, \Sigma_u^{(l)}\}$. The collapsed Gibbs structure and the procedure in [Ruggieri and Antonellis \(2016\)](#) allows us to sample and estimate first k and $V_{\tau,k}$, which are then used to sample the other parameters $\{G_0^{(l)}, G_{1:p}^{(l)}, B_0^{(l)}, B_{1:p}^{(l)}, \Sigma_{\varepsilon}^{(l)}, \Sigma_u^{(l)}\}$ given $\{k, V_{\tau,k}\}$ (steps 2 to 7). A detailed description of the posterior approximation and of the sampling methods is available in [Appendix A](#). In our application, we set $k_{\max} = 20$, $q_{ij} = 0.5$, $\eta = 100$, $\delta_{\varepsilon} = n + 2$, $\delta_u = n + 2$, $\Lambda_{\varepsilon,0} = \delta_{\varepsilon} I_n$, and $\Lambda_{u,0} = \delta_u I_n$. From our experiments, setting higher values for k_{\max} does not change the results.

3. Data Description

Our study uses daily data from Bloomberg, covering between January 28, 1999, to April 30, 2021, and includes 15 major stock market indices, including all G10 economies. We consider only one index per country, which typically contains the stock prices of the largest companies listed in the nation's largest stock exchange. The countries can be grouped into three regions: the Americas (Brazil, Canada, and the United States), Asia-Pacific (Australia, China, Hong Kong, India, Japan, and South Korea), and Europe (France, Germany, Italy, Russia, Spain, and the United Kingdom). [Table 1](#) describes the market indices chosen for the selected countries.

We report in [Figure 1](#) the daily series of closing prices on a logarithmic scale. For visualization purposes, we scale the prices to a zero mean and unit variance and add the absolute minimum value of each series to avoid negative values. This standardizes the scale of measurement for the different series.

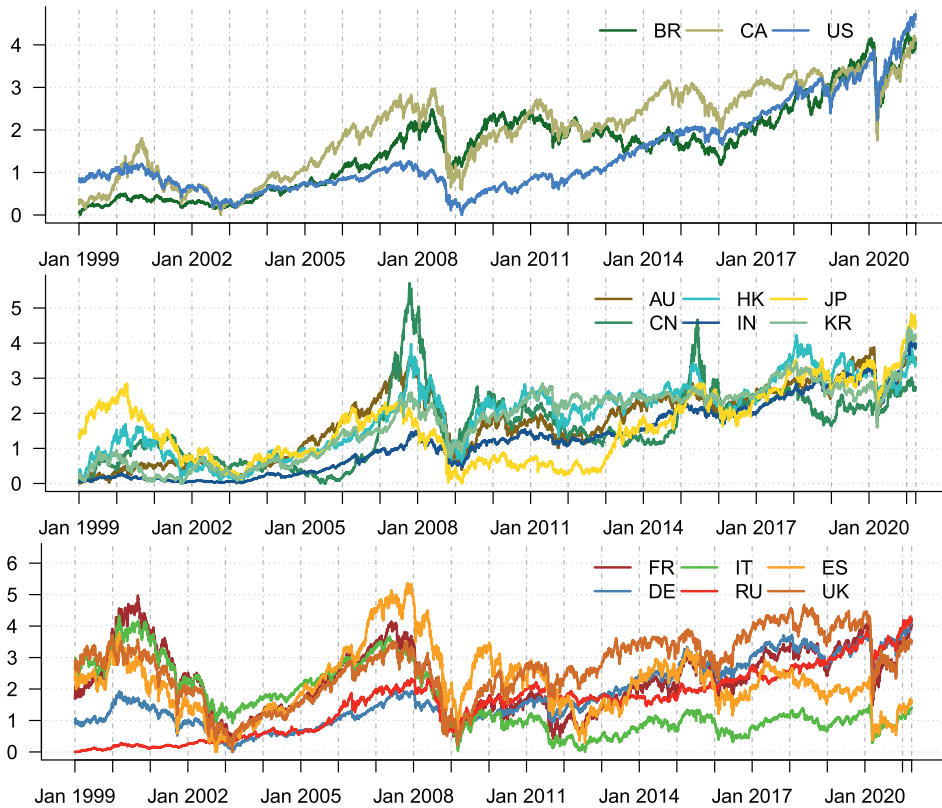


Fig. 1. Time series of daily equity log-prices from Jan-1999 to Mar-2021, by regional classification: Americas (top), Asia-Pacific (middle) and Europe (bottom).

The figure shows that global financial markets have experienced several catastrophic events within and across different markets over the past two decades. Among these events are:

1. the dotcom “tech” induced crisis of 2000–2003 which was fuelled by the adoption of the internet in the late 1990s, triggering inflated stock prices that gradually went downhill and disrupted global market operations;
2. the global financial crisis of 2007–2009 which was triggered by the massive defaults of sub-prime borrowers in the US mortgage market;
3. the European sovereign debt crisis of 2010–2013 which emanated from the inability of a cluster of EU member states to repay or refinance their sovereign debt and bailout heavily leveraged financial institutions without recourse to third party assistance;
4. and the distress to the world economy and the global financial market caused by the Covid-19 pandemic in 2020.

We compute daily returns as the log-differences of successive daily closing prices, that is, $Y_{i,t} = 100(\log C_{i,t} - \log C_{i,t-1})$, with $C_{i,t}$ the daily closing price of market i on trading day t . Table 2 reports a set of summary statistics for the index returns over the sample period. The table shows that almost all index returns have a near-zero mean and a relatively high standard deviation. The highest standard deviations, indicating individual market volatilities, are those of the emerging markets of Russia and Brazil. Almost all the return indices exhibit fairly symmetric behavior, i.e., they are characterized mostly by small but consistent positive gains and, occasionally, large negative returns. The excess kurtosis varies between 5.32 (China) and 16.78 (Canada), confirming the stylized facts of leptokurtic behavior of the daily return series.

4. Empirical Findings

4.1. Turning Points in the Global Equity Market

We select the appropriate lag of the VAR via a Bayesian information criterion (BIC) for different lag orders. The optimal lag order according minimum BIC score is $p = 1$. We report in Table 3 the number of turning points and the associated posterior probabilities. The result favors 10 turning points over the sample period considered.

Table 4 lists the turning point dates with their posterior probabilities and possible financial market events that characterize the identified dates.

Table 2

Statistics of daily returns for stock market indices over the sample period from January 28 1999 to April 30 2021.

Country	Code	Min	Max	Mean	SD	Skewness	Ex. Kurt.
Brazil	BR	-15.993	28.824	0.050	1.853	0.308	16.029
Canada	CA	-13.176	11.295	0.019	1.118	-0.902	16.868
United States	US	-12.765	10.957	0.021	1.239	-0.365	10.849
Australia	AU	-10.203	6.766	0.016	1.011	-0.705	8.481
China	CN	-9.256	9.401	0.019	1.519	-0.273	5.359
Hong Kong	HK	-13.582	13.407	0.018	1.442	-0.093	7.545
India	IN	-14.102	15.990	0.049	1.466	-0.247	9.131
Japan	JP	-12.111	13.235	0.013	1.444	-0.362	6.688
Korea	KR	-12.805	11.284	0.030	1.525	-0.454	6.403
France	FR	-13.098	10.595	0.008	1.432	-0.196	6.262
Germany	DE	-13.055	10.797	0.019	1.477	-0.162	5.687
Italy	IT	-18.541	10.874	-0.006	1.523	-0.564	8.972
Russia	RU	-20.657	25.226	0.077	2.052	-0.067	14.305
Spain	ES	-15.151	13.484	-0.002	1.464	-0.278	7.838
United Kingdom	UK	-11.512	9.384	0.002	1.188	-0.315	7.664

Table 3

Number of turning points and posterior probabilities (January 28 1999 – April 30 2021).

# of Turning Points	< 9	9	10	11	12	> 12
Posterior Probability	0	1.68×10^{-21}	1	2.15×10^{-9}	9.38×10^{-26}	0

Table 4

Turning point dates with their posterior probabilities and possible financial market events.

	Dates	Probability	Financial Market Event
1	11/09/2001	0.967	September 11 Effect
2	01/10/2001	0.997	Turn-around in Financial markets
3	08/07/2003	0.706	Turn-around after SARS induced crisis
4	23/07/2007	0.528	Panic in the asset-backed commercial paper market
5	15/09/2008	0.896	Bankruptcy of Lehman Brothers
6	06/11/2008	0.976	IMF prediction of deep recession
7	07/07/2009	0.945	End of the great recession
8	12/07/2016	0.584	Rising oil prices and Aftermath of Brexit
9	21/02/2020	0.999	Beginning of Covid-19 induced a global stock market crash
10	08/04/2020	0.921	End of Covid-19 induced a global stock market crash

The first turning point (event #1) in the financial market over the past two decades is the September 11, 2001 attack that led to one of the most significant single-day point declines in major markets. A turn-around followed this at the beginning of October 2001 (event #2). We shall notice that the number of samples between the first and second turning point is relatively small, about 20. In this case, the sparse graphical prior proposed in [Ahelegbey et al. \(2016b\)](#) can be applied in combination with turning point prior distributions. We leave this topic for future research.

The Severe Acute Respiratory Syndrome (SARS) outbreak timeline shows that the illness first appeared in Guangdong Province, China, in November 2002 and spread to 37 countries. This affected the Asian financial market and began to affect stock market integration around early 2003. The World Health Organisation (WHO) database shows that the SARS infection period was from 16/11/2002 – 05/07/2003 ([see Organization, 2003](#)). Thus, the third turning point (event #3) captures the turn-around in the financial market due to WHO's declaration that SARS outbreaks have been contained worldwide.

The fourth turning point (event #4) marks the contraction in the asset-backed commercial paper (ABCP) market that began in late July 2007, which triggered fears and panic across the financial market. As documented by [Covitz et al. \(2013\)](#) and in [Commission \(2011\)](#), the collapse of the ABCP market played a central role in transforming concerns about the credit quality of mortgage-related assets into a global financial crisis. Early July 2007 also experienced the collapse of two Bear Stearns hedge funds that had speculated heavily in mortgage-backed securities.

The fifth turning point (event #5) marks September 15, 2008, when stock markets experienced the worst sell-off in the last 20 years. It was a Monday that followed a weekend turmoil of triple trouble. That is, Lehman Brothers (the fourth-largest US investment bank at the time) filed for Chapter 11 bankruptcy protection; Bank of America acquired Merrill Lynch, and the American International Group (AIG - the world's largest insurance company) presented an unprecedented request for short-term financing from the Federal Reserve. According to the [Commission \(2011\)](#), the risk exposures of AIG are concentrated among the largest international banks (both US and European) across a wide array of product types (e.g., bank lines, derivatives, securities lending). Thus, AIG's failure could trigger significant counterparty losses to these firms. The fears and

panic across financial markets led to increased interconnectedness which amplified the shocks, affecting a broader aspect of the US financial system and many other correlated markets and economies.

By the end of October 2008, many advanced economies like the US, Europe, and Japan were already facing their deepest recession since the 1930s. With the global financial market in turmoil, producers and consumers were losing confidence in the financial system. As documented in the World Economic Outlook report published on November 6th, 2008 (see IMF, 2008), the IMF predicted a worldwide “deep recession” in 2009 following the deteriorated global growth of world GDP over the past month. This forecast, coupled with financial conditions, continued to present serious downside risks, pushing the world over the edge with reaction across major stock markets. Thus, the sixth turning point (event #6) marks the date of the IMF prediction with its effect on the global equity market.

The seventh turning point (event #7) identifies July 7th, 2009 as the day that marks the beginning of the global economic recovery from the great recession. In its World Economic Outlook report published on July 8th, 2009 (see IMF, 2009), the IMF projected receding contractionary forces with a positive but weak recovery between 2009–2010.

Rising crude oil prices in July 2016 affected oil-producing countries and oil-dependent nations, sending market participants worried about the possible impact of rising crude oil prices on the global stock market activities. The period also coincides with the aftermath of the Brexit, which saw Britain voting to exit the EU in June 2016. The uncertainty surrounding Brexit had a significant effect on many investors, thereby altering financial market activities across the globe. The failure of the Bank of England to ease the shocks that followed the Brexit vote also contribute to a mild turning point (i.e., event #8).

Discussions of the first Covid-19 case date back to mid-November 2019. A global pandemic was triggered when the severity and scale of the impact of the novel Coronavirus led to what can be best described as “hibernation” of world activities, i.e., a temporary sleep or “artificial coma”. February 21st, 2020 (event #9) marked the day Covid-19 outbreak began to affect Europe and the US, plunging many stock markets into turmoil. Despite its impact, the GFC is incomparable to the Covid-19 outbreak regarding the scale and magnitude of its effects. The uncertainty at the onset of the latter was accompanied by the existential threat from which many markets may not recover in the sense that it could cripple if not wipe out nations and economies completely. This assertion is evidence by the fact that it recorded the fastest fall in the global stock market (see Figure 1). Unlike any of the past crises, within just a month of reported Covid-19 cases in Europe and the US, major national indices began to record their worst ever historical prices in history.

The last turning point (event #10) marks the beginning of financial market recovery from the Covid-19 outbreak. Although the global stock market is in a recovery phase, major world economies are currently in a recession or depression.

4.2. Structural Dynamic Interconnectedness in the Global Equity Market

A preliminary analysis of the equity market return provides some evidence in favor of some variations and sudden changes in the level of interconnectedness. More specifically, we estimate connectedness via yearly rolling windows of 240 trading days. We monitor the daily changes in interconnectedness by setting the increments between successive rolling windows to one day. Thus, we set the first window of our study from January 28, 1999, to January 3, 2000, followed by January 29, 1999, to January 4, 2000; the last window is from March 31, 2020, to April 30, 2021. In total, we consider 5426 rolling windows. We used the data points of April 2021 to test the out-of-sample forecast performance of our model.

Various measures of connectedness have been proposed in the literature (e.g., see Acharya et al., 2010; Adrian and Brunnermeier, 2016). Our change point BGVAR model and the Bayesian estimator for large covariance matrices can be used to compute measures based on covariance matrices and their eigenvalues following for example Billio et al. (2012) and Massacci (2017, 2021). Nevertheless, since our BGVAR model naturally provides a network representation of the lagged and contemporaneous dependence among time series, we focus on network-based measures. We estimate two well-known measures: the network density (Billio et al., 2012), which exploits the notion of Granger's causality among time series, and the spillover index (Diebold and Yilmaz, 2014) which relies on the Sims' causality notion. See Eichler (2013) for a review of causality in multiple time series.

The Network Density measure is computed from the restrictions on the autoregressive coefficient matrix:

$$\text{Network Density}(A^{(l)}) = \frac{100}{n(n-1)} \sum_{i=1}^n \sum_{j=1}^n A_{ij}^{(l)}. \quad (8)$$

The Spillover Index is computed from the autoregressive coefficient matrix and the covariance matrix through the generalized forecast error variance decomposition:

$$\text{Spillover Index}(B^{(l)}, \Sigma_u^{(l)}; H) = \frac{100}{n} \sum_{ij=1, i \neq j}^n \left(\frac{S_{ij}(B^{(l)}, \Sigma_u^{(l)}; H)}{\sum_{j=1}^n S_{ij}(B^{(l)}, \Sigma_u^{(l)}; H)} \right), \quad (9)$$

where

$$S_{ij}(B^{(l)}, \Sigma_u^{(l)}; H) = \frac{\sigma_{jj,u}^{(l)-1} \sum_{r=0}^{H-1} (e_i' \theta_r^{(l)} \Sigma_u^{(l)} e_j)^2}{\sum_{r=0}^{H-1} (e_i' \theta_r^{(l)} \Sigma_u^{(l)} \theta_r^{(l)'} e_i)},$$

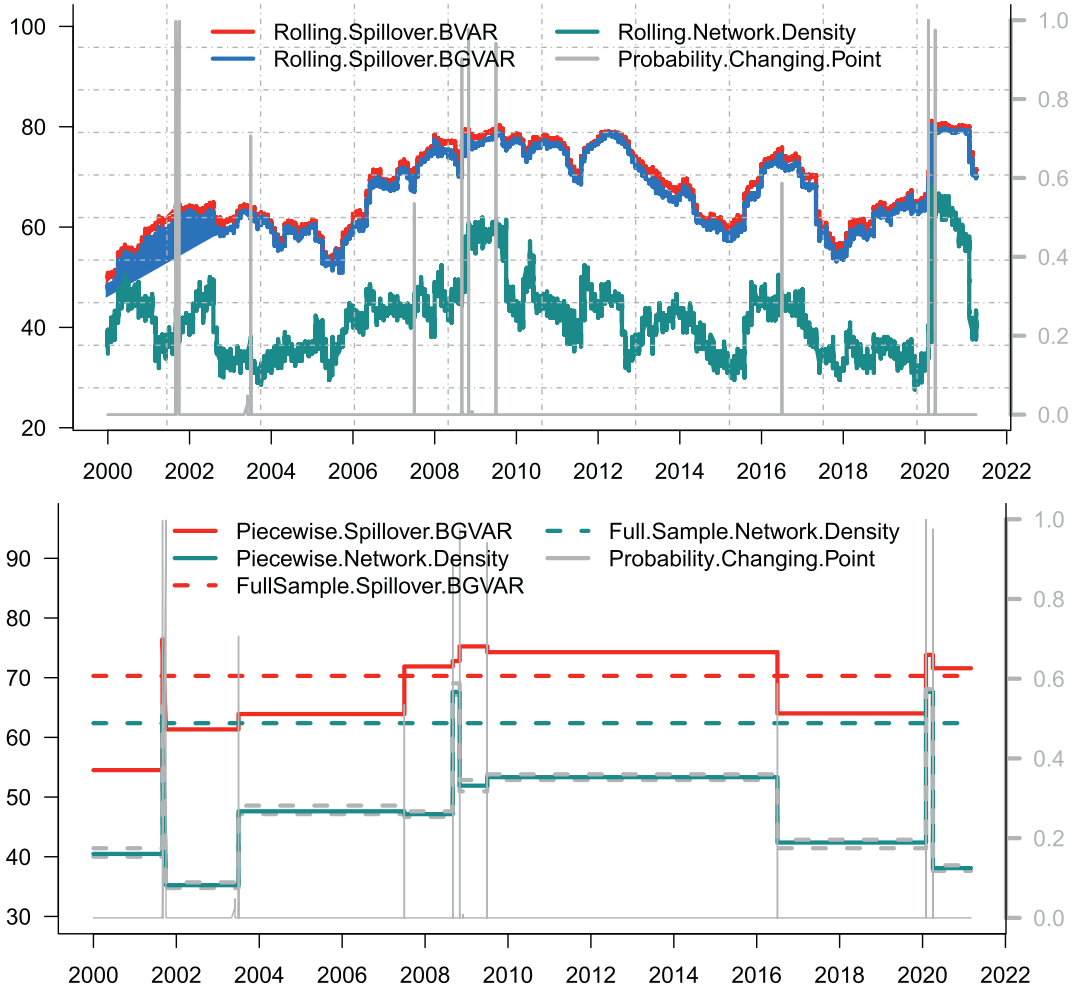


Fig. 2. Top: rolling-window estimates of the Spillover index following BVAR and BGVAR models and the estimate the Network Density. Bottom: Spillover index following BGVAR with change points and Network density, both on the entire sample (solid lines) and on subsamples (dashed lines). In all plots: the posterior probability of turning points (gray line).

with $\theta_r^{(l)} = B_1^{(l)}\theta_{r-1}^{(l)} + B_2^{(l)}\theta_{r-2}^{(l)} + \dots + B_p^{(l)}\theta_{r-p}^{(l)}$, with $\theta_0^{(l)} = I_n$ and $\theta_r^{(l)} = 0$ for $r < 0$. The upper-script l indicates sub-periods, $A_{ij}^{(l)}$ is defined in (5), H is the number of steps ahead forecast, e_j is the j -th element of the standard orthonormal basis of \mathbb{R}^n , $B_1^{(l)}$ is the autoregressive coefficient matrix, $\Sigma_u^{(l)}$ is the covariance matrix defined in (3), and $\sigma_{j,u}^{(l)}$ is the j -th diagonal element of $\Sigma_u^{(l)}$. The unknown parameters used in the calculation of the connectedness measures are replaced by the corresponding estimates. Concerning the adjacency matrix $A^{(l)}$ of the BGVAR, a MAP estimator is considered for the entries of the matrix.

We report in Figure 2 the plot of rolling-window and piecewise Network Density and Spillover index from the standard Bayesian VAR (BVAR) and the Bayesian graphical VAR (BGVAR) together with the posterior probability of a turning point for each day between January 3, 2000, to March 31, 2021.

The figure shows that the network density and spillover index of the global financial crisis (GFC) and Covid-19 periods are much greater than any period of market crisis in the last 20 years, and this includes the period of the dot-com “tech” induced crisis of 2000–2003, and the European sovereign debt crisis of 2010–2013. The spike in the network density and spillover index after February 2020 is typified by the fear and panic that greeted the global financial market, thus intensifying sell-off assets.

According to [Forbes and Rigobon \(2002\)](#), when markets exhibit a high degree of comovement during periods of stable economic/financial conditions, and these continue to be highly correlated after a shock. The markets are said to be inter-dependent and do not constitute contagion. However, when there is a significant increase in cross-market linkages after a shock to one/more markets, this suggests contagion. The increased interconnectedness during 2008–2009 and 2020 provides

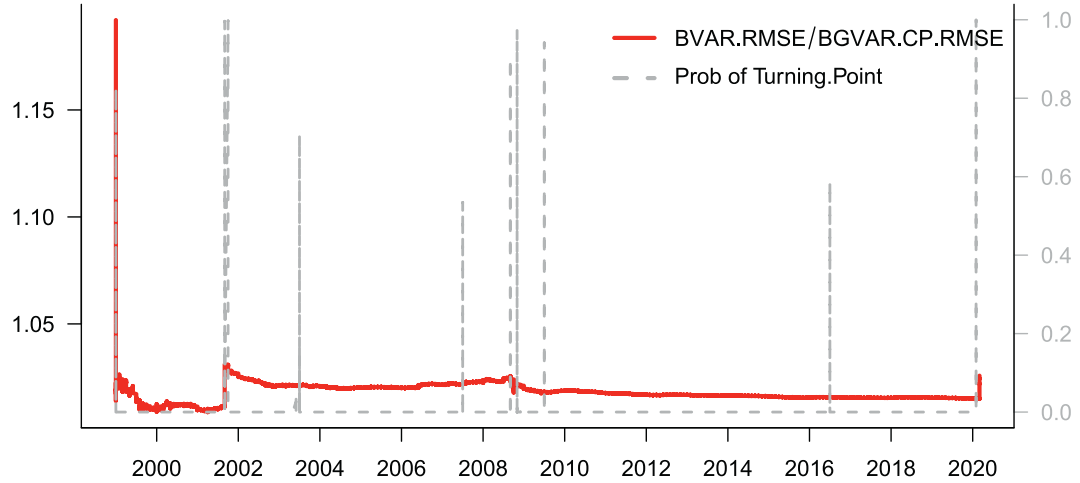


Fig. 3. Ratio between BVAR and BGVAR-CP root mean square errors (red solid line) and turning points posterior probability (dashed line).

Table 5
Out-of-sample RMSFE of the point forecast performance of BVAR and BGVAR-CP model.

	Minimum	Maximum	Mean	Std-Deviation
BVAR	0.0697	18.1375	1.6422	2.1843
BGVAR-CP	0.0211	16.3338	1.5981	2.0663

more substantial evidence of contagion in the global financial crisis and Covid-19 pandemic than during the dot-com and Eurozone crises.

A closer look at the rolling spillover index from the BVAR and BGVAR in Figure 2 suggests an insignificant difference between the spillover from both models. This can be attributed to the fact that the generalized forecast error variance decomposition assumes a full error covariance structure, which means the variables in the model are contemporaneously interdependent. Thus, the difference between the two indices is due to the sparsity in the autoregressive coefficients matrix of the BGVAR model.

We report in Figure 3 the results of the comparison between the BVAR and the BGVAR change-points (BGVAR-CP) model using the ratio of the root-mean-squared-errors (RMSE).

Figure 3 reports the ratio between the root-mean-squared-error (RMSE) for the BVAR and the BGVAR change-points (BGVAR-CP) model. When the ratio of RMSE is greater than 1, then the BGVAR-CP model is preferred to the BVAR in terms of predictive performance. Over the sample period considered, the ratio of the RMSEs ranged between 1.009 – 1.192, with an average value of 1.018 and a standard deviation of 0.01. Thus, the BGVAR-CP achieved higher predictive accuracy than the BVAR.

We report in Table 5 the out-of-sample root-mean-squared forecast error of the performance of the BVAR and the BGVAR-CP model. The result again favour the the BGVAR-CP over the BVAR.

4.3. Dynamic Interconnectedness in the Global Equity Market

We analyze the dynamic nature of the interconnectedness among the major stock markets. Using the turning point dates estimated with our change-point BGVAR model, we divide the sample into four sub-periods of tranquil and turbulent times: (03/01/2000 – 12/09/2008), (15/09/2008 – 06/07/2009), (07/07/2009 – 20/02/2020), and (21/02/2020 – 31/03/2021). In each sub-period l the graph adjacency matrix $A_{ij}^{(l)}$ is the union graph of the contemporaneous and lagged dependence graphs, $G_0^{(l)}$ and $G_1^{(l)}$, respectively. The entries of $G_s^{(l)}$ are MAP estimates based on the edge posterior probability. We report in Figure 4 the network topology over the sub-periods. Each network is represented with color-coded links and nodes. Red links indicate negative weights, and green links denote positive weights. Red-color nodes represent American markets, blue nodes for European markets, and green nodes for markets in Asia-Pacific countries. The size of the nodes is proportional to their hub scores.

The figure provides strong evidence of clustering among the markets. More importantly, the Asian-Pacific markets (green-nodes) seem to move together, likewise, the European markets (blue-nodes) due to similarities in underlying market conditions. The US, however, appears separated from the others most of the time, as the rest of the American markets (red-nodes) are usually closer to the European ones. We notice that the US is usually the biggest sized node and strongly positively connected to the rest of the markets. Based on the node sizes, the US appears to be the most influential in almost all the

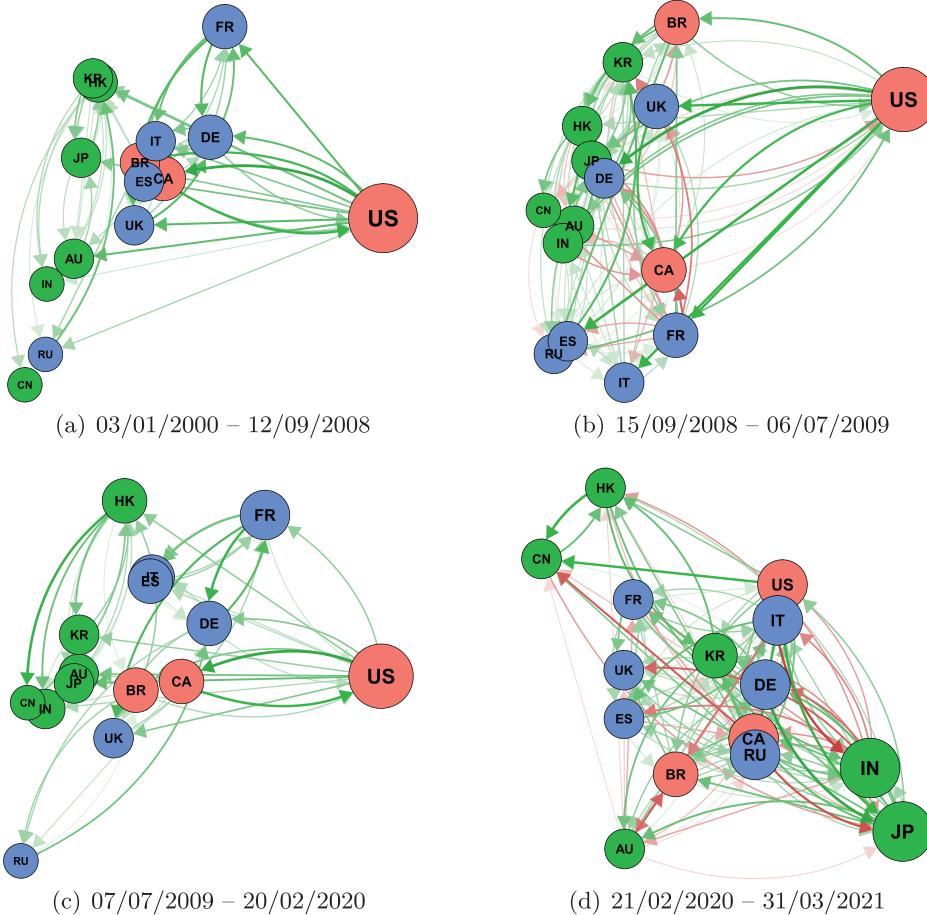


Fig. 4. Sub-period Interconnectedness. Red nodes represent America markets, blue for European, and green for Asia-Pacific. The size of the nodes are weighted out-degree. Red links denote negative effects and green for positive interactions. The node position is based on eigendecomposition of the networks. Note: the graph adjacency matrix $A_{ij}^{(l)}$ is the union graph of the contemporaneous and lagged dependence graphs, $G_0^{(l)}$ and $G_1^{(l)}$, respectively. The entries of $G_s^{(l)}$ are MAP estimates based on the edge posterior probability.

Table 6

Statistics of the networks in the sub-periods both estimated with our change-point BVAR model. Note: the graph adjacency matrix $A_{ij}^{(l)}$ is the union graph of the contemporaneous and lagged dependence graphs, $G_0^{(l)}$ and $G_1^{(l)}$, respectively. The entries of $G_s^{(l)}$ are MAP estimates based on the edge posterior probability.

No.	Date Interval	Average Degree	Density	Clustering Coefficient	Average Path Length
1	03/01/2000 – 12/09/2008	4.000	28.571	0.597	1.903
2	15/09/2008 – 06/07/2009	8.133	58.095	0.749	1.419
3	07/07/2009 – 20/02/2020	4.133	29.524	0.532	2.171
4	21/02/2020 – 31/03/2021	8.667	61.905	0.830	1.424

sub-periods except 21/02/2020 – 31/03/2021, where Japan seems to dominate. Thus, the results suggest that before the Covid-19 outbreak, the US equity market significantly impacted other markets, reflecting its leadership and influence in the equity market.

Since spillover transmission can involve markets that are connected directly or indirectly through other markets, we compare the sub-period networks in terms of direct connectivity measures (average degree, density), local indirect connectivity (clustering coefficient), and global indirect connectivity (average path length). See Appendix B for a description of these network metrics. Table 6 shows that network statistics extracted for the four sub-period connectivity structures. We notice that two sub-periods record tranquil (non-crisis) conditions (i.e., 03/01/2000 – 12/09/2008 and 07/07/2009 – 20/02/2020), while the other two (15/09/2008 – 06/07/2009, and 21/02/2020 – 31/03/2021) experienced stressful conditions. The tranquil periods are characterized by a relatively low average degree of interconnectedness, lower density, and clustering index, and a relatively high average path length. This suggests a lower degree of equity market integration before and after the global

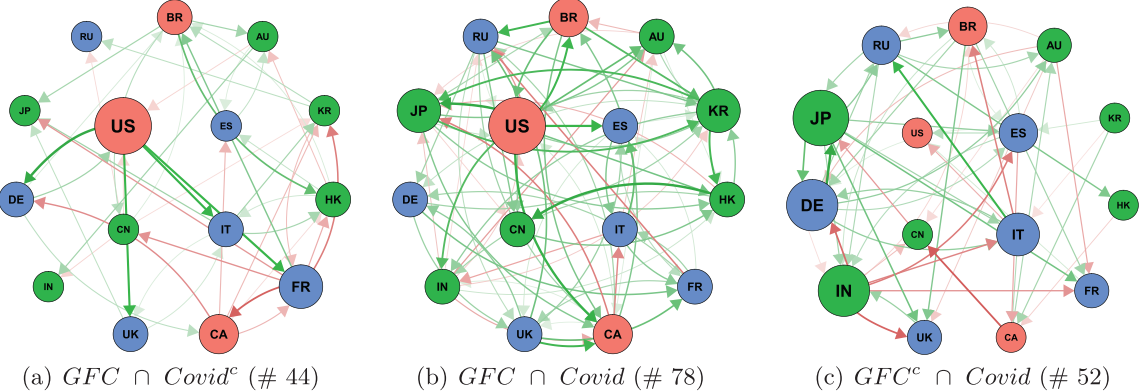


Fig. 5. Comparing the Global Financial Crisis network (GFC) and Covid-19 outbreak network. Red nodes represent America markets, blue for European, and green for Asia-Pacific. The size of the nodes are weighted out-degree. Red links denote negative effects and green for positive interactions. The number in parenthesis signifies the total links in each network. Note: G^c denotes the complement of the graph G . The graph adjacency matrix $A_{ij}^{(l)}$ is the union graph of the contemporaneous and lagged dependence graphs, $G_0^{(l)}$ and $G_1^{(l)}$, respectively. The entries of $G_s^{(l)}$ are MAP estimates based on the edge posterior probability.

Table 7
Centrality ranking during the Global Financial Crisis and the Covid-19 Pandemic.

Rank	GFC (2008–2009)				Covid (2020)			
	Hub	Authority		Hub	Authority			
1	US	0.774	CA	0.406	IN	0.395	JP	0.355
2	FR	0.331	DE	0.356	JP	0.389	AU	0.327
3	UK	0.259	FR	0.309	DE	0.352	RU	0.325
4	BR	0.250	ES	0.292	US	0.349	IN	0.294
5	CA	0.227	IT	0.286	IT	0.332	CA	0.282
6	IT	0.166	JP	0.263	CA	0.328	BR	0.251
7	KR	0.159	KR	0.262	RU	0.224	KR	0.251
8	HK	0.116	UK	0.255	KR	0.209	UK	0.242
9	JP	0.110	HK	0.236	FR	0.198	DE	0.232
10	AU	0.089	BR	0.223	ES	0.175	ES	0.227
11	DE	0.086	IN	0.213	BR	0.167	FR	0.223
12	IN	0.072	RU	0.181	HK	0.131	US	0.211
13	RU	0.067	CN	0.169	UK	0.119	IT	0.209
14	ES	0.063	AU	0.165	AU	0.079	CN	0.196
15	CN	0.054	US	0.067	CN	0.027	HK	0.172

financial crisis. It also shows that in the event of a shock to a major market or a group of major markets, this shock will take a much longer time to propagate to other markets to cause a systemic breakdown.

On the other hand, the turbulent periods are characterized by a relatively high average degree of interconnectedness, a high density and clustering index, and a relatively low average path length. The lower average path length shows that it takes a relatively shorter time for a shock to a major market or a group of major markets to propagate to other markets, leading to a systemic breakdown. The network statistics of 15/09/2008 – 06/07/2009 and 21/02/2020 – 31/03/2021 periods show that stock market integration during the GFC is strikingly similar to the behavior exhibited most recently at the height of the Covid-19 pandemic in 2020. More importantly, the spikes in the network density at the onset of both crisis periods (see Figure 2) indicate elevated levels of unusualness in stock markets with a rise in volatility and market co-movements.

4.4. Global Financial Crisis vs Covid-19 Outbreak

We compare the interconnectedness of markets during the GFC and the Covid-19 outbreak. For this comparison, we extract the intersection and differences between the networks. Figure 5 presents the similarity and differences between the structure of interconnectedness during the GFC and Covid-19 sub-periods. Figure 5(a) depicts the network links during the GFC but not in the Covid-19 period. Figure 5(b) display the network links common to both periods, and Figure 5(c) shows only links in the Covid-19 period but not present during the GFC.

Overall, we found 78 common connections between both networks. The GFC recorded 44 extra links that were not present in the Covid-19 network, and the latter also report 52 new connections that were not in existence during the

financial crisis. Surprisingly, the majority of the new stock market connections center around Japan, Germany, and India, whereas the GFC period centered around the US.

We now turn our attention to assess and compare the most critical (or central) market during what appears to be the two most severe equity market crises over the last two decades. Table 7 reports the summary of the centrality ranking of the most influential markets over the two crisis sub-periods. The top three transmitters (e.g. high hub scores) of spillover propagation during the GFC are the US, France, and UK, while the top three receivers of shocks during the period were Canada, Germany, and France. During the Covid-19 outbreak, most central markets in transmitting shocks are India, Japan, and Germany, while Japan, Australia, and Russia rank high at the receiving shocks. Thus, not only has the structure of the nature of interconnectedness changed over the two crisis, but the most central markets for spillover propagation has also changed in recent times.

5. Conclusion

This paper studies the nature of the turning points in financial equity markets. We propose a Bayesian technique for turning point detection in a piece-wise network vector autoregressive model that approximates the interconnectedness among stock market returns. The empirical application examines turning points in the global equity market over the past two decades. We also compare the Covid-19 induced interconnectedness with that of the global financial crisis to identify similarities and the most central markets for spillover propagation.

Our proposed approach proves to be effective in identifying financial market turning points in relevant periods, like the September 11 attack of 2001, the turn-around after SARS induced crisis in 2003, the panic in the asset-backed commercial paper market in 2007, the Bankruptcy of Lehman Brothers in 2008, the beginning and the end of 2008–2009 great recession, the rising oil prices and aftermath of Brexit in 2016, and the beginning and end of Covid-19 induced global stock market crashed in 2020. We document a significant change in the structure of stock market integration during the global financial crisis and the Covid-19 outbreak. The result shows that the Covid-19 induced market interconnections record the highest network density, suggesting stronger evidence of spillovers and contagion in the Covid-19 outbreak than during the global financial crisis.

Acknowledgements

MB and RC acknowledge financial support from the Italian Ministry MIUR under the PRIN project Hi-Di NET - Econometric Analysis of High Dimensional Models with Network Structures in Macroeconomics and Finance (grant agreement no. 2017TA7TYC) and from the Venice Centre for Risk Analytics (VERA) at the Ca' Foscari University of Venice.

Appendix A. Details of Posterior Approximation and Sampling Approach

A1. Posterior Approximation

Let $Z_t = (Y'_t, Y'_{t-1}, \dots, Y'_{t-p})'$ be m -dimensional vector of contemporaneous and lagged observations, where $m = n(p+1)$. Denote with $Z^{(l)} = (Z_{\tau_{l-1}+1}, \dots, Z_{\tau_l})$ is $h \times m$ matrix of the observations Z_t with t in the time interval $(\tau_{l-1}, \tau_l]$ of length $h = \tau_l - \tau_{l-1}$. For some lag order p , and under the assumption that $Z_{1:h} \sim \mathcal{N}(0, \Sigma^{(l)})$, the likelihood function is given by

$$P(Z^{(l)} | \Sigma^{(l)}) = (2\pi)^{-\frac{mh}{2}} |\Sigma^{(l)}|^{-\frac{h}{2}} \text{etr}\left(-\frac{1}{2}\Sigma^{(l)-1}\hat{S}^{(l)}\right), \quad (\text{A.1})$$

where $\text{etr}(\cdot)$ is the exponential of the standard trace function, $\hat{S}^{(l)} = \sum_{t=\tau_{l-1}+1}^{\tau_l} Z_t Z_t'$ is the sample sum of squared matrix of dimension m . It can be shown that $\Sigma^{(l)}$ is a transform of the structural parameters $(B^{(l)}, \Sigma_\varepsilon^{(l)})$ (see Ahelegbey et al., 2016b, section 2). Under the assumption that $\Sigma^{(l)}$ is inverse-Wishart distributed, $P(\Sigma^{(l)}) \sim \mathcal{IW}(\nu, \Lambda)$, with prior expectation $\frac{1}{\nu} \Lambda$ and $\nu > m$ degrees of freedom, we follow the Bayesian framework of Geiger and Heckerman (2002) to integrate out the structural parameters analytically, thus, obtaining a marginal likelihood function given by

$$P(Z^{(l)}) = \frac{(\pi)^{-\frac{mh}{2}} (\nu)^{\frac{mv}{2}}}{(\nu + h)^{\frac{m}{2}(\nu+h)}} \prod_{i=1}^m \frac{\Gamma\left(\frac{\nu+h+1-i}{2}\right)}{\Gamma\left(\frac{\nu+1-i}{2}\right)} |\bar{\Sigma}^{(l)}|^{-\frac{1}{2}(\nu+h)}, \quad (\text{A.2})$$

where $\bar{\Sigma}^{(l)} = (\Lambda + \hat{S}^{(l)})/(\nu + h)$ is the posterior covariance matrix. Clearly, we can notice that h controls the window size which is related to the turning point locations. From the above representation, we notice that except for $\bar{\Sigma}^{(l)}$ whose computation depends on the observed data, the rest can be pre-computed for different values of h , $1 \leq h \leq T$ with $\nu = m + 2$.

This allows us to apply an efficient sampling algorithm to sample the model parameters in blocks. The algorithm proceeds as follows:

1. Sample $[k, V_{\tau,k}|Y, p]$ following Ruggieri and Antonellis (2016) by:
 - (a) sampling k from the marginal distribution: $[k|Y]$;

- (b) recursively sampling $V_{\tau,k}$ from the conditional distribution: $[V_{\tau,k}|k, Y]$.
2. For $l = 1, \dots, k+1$, sample $[G_0^{(l)}, G_{1:p}^{(l)}, B_0^{(l)}, B_{1:p}^{(l)}, \Sigma_{\varepsilon}^{(l)}, \Sigma_u^{(l)}|Y, p, k, V_{\tau,k}]$ as follows:
- Sample via a Metropolis-within-Gibbs $[G_0^{(l)}, G_{1:p}^{(l)}|Y, p, k, V_{\tau,k}]$ by:
 - sampling $G_{1:p}^{(l)}$ from the marginal distribution: $[G_{1:p}^{(l)}|Y, p, k, V_{\tau,k}]$;
 - sampling $G_0^{(l)}$ from the conditional distribution: $[G_0^{(l)}|Y, p, G_{1:p}^{(l)}, k, V_{\tau,k}]$.
 - Sample from $[B_0^{(l)}, B_{1:p}^{(l)}, \Sigma_{\varepsilon}^{(l)}, \Sigma_u^{(l)}|Y, G_0^{(l)}, G_{1:p}^{(l)}, p, k, V_{\tau,k}]$ by iterating the following steps.

- Draw $[B_{i,\pi_i|1:p}^{(l)}|Y, G_{1:p}^{(l)}, G_0^{(l)}, B_{1:p}^{(l)}, \Sigma_{\varepsilon}^{(l)}, \Sigma_u^{(l)}] \sim \mathcal{N}(\bar{B}_{i,\pi_i|1:p}^{(l)}, D_{\pi_i}^{(l)})$, where

$$\bar{B}_{i,\pi_i|1:p}^{(l)} = \sigma_{u,i}^{-2} D_{\pi_i}^{(l)} Z'_{\pi_i} Y_i, \quad D_{\pi_i}^{(l)} = (\eta^{-1} I_{d_z} + \sigma_{u,i}^{-2} Z'_{\pi_i} Z_{\pi_i})^{-1}, \quad (\text{A.3})$$

where $Z_{\pi_i} \in Z$ corresponds to $(G_{y_i, z_{\pi_i}|1:p}^{(l)} = 1)$, $\sigma_{u,i}^2$ is the i -th diagonal element of $\Sigma_u^{(l)}$, d_z is the number of covariates in Z_{π_i} , and π_i is the parent node set defined by $\pi_i = \{j = 1, \dots, np, \text{ s.t. } G_{ij|1:p}^{(l)} = 1\}$.

- Draw $[B_{i,\pi_i|0}^{(l)}|Y, G_0^{(l)}, G_{1:p}^{(l)}, B_{1:p}^{(l)}, \Sigma_{\varepsilon}^{(l)}, \Sigma_u^{(l)}] \sim \mathcal{N}(\bar{B}_{i,\pi_i|0}^{(l)}, Q_{\pi_i}^{(l)})$, where

$$\bar{B}_{i,\pi_i|0}^{(l)} = \sigma_{\varepsilon,i}^{-2} Q_{\pi_i}^{(l)} \hat{U}_{\pi_i}^{(l)'} \hat{U}_i^{(l)}, \quad Q_{\pi_i}^{(l)} = (\eta^{-1} I_{d_u} + \sigma_{\varepsilon,i}^{-2} \hat{U}_{\pi_i}^{(l)'} \hat{U}_{\pi_i}^{(l)})^{-1} \quad (\text{A.4})$$

with $\hat{U}^{(l)} = Y - Z B_{1:p}^{(l)'}, \hat{U}_{\pi_i}^{(l)} \in \hat{U}_{-i}^{(l)}$ is the contemporaneous predictors of $\hat{U}_i^{(l)}$ that corresponds to $(G_{y_i, y_{\pi_i}|0}^{(l)} = 1)$, d_u is the number of covariates in $\hat{U}_{\pi_i}^{(l)}$, and π_i is the parent node set defined by $\pi_i = \{j = 1, \dots, n, \text{ s.t. } G_{ij|0}^{(l)} = 1\}$.

- Draw $[\Sigma_{\varepsilon}^{(l)-1}|Y, G_{1:p}^{(l)}, G_0^{(l)}, B_{1:p}^{(l)}, B_0^{(l)}, \Sigma_u^{(l)}] \sim \mathcal{W}_G(\delta_{\varepsilon} + N, \Lambda_{\varepsilon,N})$ where

$$\Lambda_{\varepsilon,N} = \Lambda_{\varepsilon,0} + \hat{\varepsilon}^{(l)'} \hat{\varepsilon}^{(l)}, \quad \hat{\varepsilon}^{(l)} = \hat{U}^{(l)} - \hat{U}^{(l)} B_0^{(l)'} \quad (\text{A.5})$$

- Draw $[\Sigma_u^{(l)-1}|Y, G_{1:p}^{(l)}, G_0^{(l)}, B_{1:p}^{(l)}, B_0^{(l)}, \Sigma_{\varepsilon}^{(l)}] \sim \mathcal{W}(\delta_u + N, \Lambda_{u,N})$ where

$$\Lambda_{u,N} = \Lambda_{u,0} + \hat{U}^{(l)'} \hat{U}^{(l)}. \quad (\text{A.6})$$

A2. Sampling Approach of the Parameters

This section provides a detailed description of the sampling approach of the parameters.

A3. Sampling Number of Turning Points

Using Bayes rule, the posterior distribution on the number of turning points is given as:

$$\begin{aligned} P(K = k|Z) &= \frac{P(K = k)P(V_{\tau,k}|K = k)P(Z|K = k, V_{\tau,k})}{P(Z)} \\ &= \frac{1}{k_{\max} + 1} \frac{1}{N_k} \frac{P(Z|K = k, V_{\tau,k})}{P(Z)}, \end{aligned} \quad (\text{A.7})$$

where

$$P(Z) = \sum_k \sum_{V_{\tau,k}} P(Z|K = k, V_{\tau,k})P(K = k, V_{\tau,k}). \quad (\text{A.8})$$

Let $Z_{1:h} = (Z_1, \dots, Z_h)$. For $t = 1, \dots, T$, we denote with $\Psi_k(1, h) = P(Z_{1:h}|K = k, V_{\tau,k})$, the density of $Z_{1:h}$ with $k > 0$ turning points defined by (see Ruggieri, 2013)

$$\Psi_k(1, h) = \sum_{t < h} \Psi_{k-1}(1, t)P(Z_{t+1:h}), \quad (\text{A.9})$$

for $h = (kd_{\tau} + 1), \dots, T$, where the above density for $k = 0$ is initialized by $\Psi_0(1, t) = P(Z_{1:t})$, and $d_{\tau} = \tau_l - \tau_{l-1}$ is the distance between two successive turning points.

A4. Sample Turning Point Locations

Following the process of filtering recursion (see Fearnhead, 2006; Ruggieri, 2013), the posterior distribution of the first turning point is given by

$$P(\tau_1 = s|Z) = \frac{\Psi_0(1, s) P(Z_{s+1:T})}{\sum_{s < T} \Psi_0(1, s) P(Z_{s+1:T})}, \quad (\text{A.10})$$

and the posterior distribution of the first turning point is given by

$$P(\tau_k = t | \tau_{k+1}, Z) = \frac{\Psi_{k-1}(Z_{1:t}) P(Z_{t+1:\tau_{k+1}})}{\sum_{t \in [k-1, \tau_{k+1}]} \Psi_{k-1}(Z_{1:t}) P(Z_{t+1:\tau_{k+1}})}. \quad (\text{A.11})$$

A5. Sampling The Network

Let $V_y = (y_1, \dots, y_n)$ be the vector of indices of response variables, and $V_z = (z_1, \dots, z_{np})$ the indices of the lagged observations. The network relationship from $z_\psi \in V_z$ to $y_i \in V_y$ can be represented by ($G_{y_i, z_\psi} = 1$). Following Geiger and Heckerman (2002), the closed-form expression of the local marginal likelihood is given by

$$P(Y|G_{y_i, z_\psi}) = \frac{\pi^{-\frac{1}{2}N} v_0^{\frac{1}{2}v_0} \Gamma\left(\frac{v_0+N-n_x}{2}\right)}{v_n^{\frac{1}{2}v_n} \Gamma\left(\frac{v_0-n_x}{2}\right)} \left(\frac{|Z'_\psi Z_\psi + v_0 I_{n_\psi}|}{|X'_i X_i + v_0 I_{n_x}|} \right)^{\frac{1}{2}v_n}, \quad (\text{A.12})$$

where $\Gamma(\cdot)$ is the gamma function, $X_i = (Y_i, Z_\psi)$, I_d is a d -dimensional identity matrix, n_ψ is the number of covariates in Z_ψ , $n_x = n_\psi + 1$, $v_0 > n_x$ is a degree of freedom hyper-parameter of the prior precision matrix of (Y, Z) , and $v_n = v_0 + N$. Equation (A.12) indicates that only the ratio of the posterior sum of squares depend on the data. Thus, we reduce computational time by pre-computing the part of () that is independent of the data, for different values of $n_x \in [1, m]$ and for fixed $v_0 = m + 2$ and N . We also pre-compute the posterior of the full sum of squares matrix and extract the sub-matrices that relates to $\{Z_\psi\}$ and $\{(Y_i, Z_\psi)\}$. For computational details of the score function (see Ahelegbey et al., 2016a). See Algorithms 1 and 2 for a pseudo code of the lagged and contemporaneous network sampling steps.

Algorithm 1 Sampling $[G_{1:p}|Y, p]$

- 1: **Require:** Set of responses $V_y = (y_1, \dots, y_n)$ and lagged attributes $V_z = (z_1, \dots, z_{np})$
 - 2: Initialize $G_{1:p}^{(1)} = \emptyset$
 - 3: **for** $y_i \in V_y$ **do**
 - 4: **for** $z_j \in V_z$ **do**
 - 5: Compute $\phi_a = P(Y|G_{y_i, \emptyset|1:p}^{(1)})$ and $\phi_b = P(Y|G_{y_i, z_j|1:p}^{(1)})$
 - 6: **if** $\phi_b > \phi_a$ **then** $G_{y_i, z_j|1:p}^{(1)} = 1$ **else** $G_{y_i, z_j|1:p}^{(1)} = 0$
 - 7: **for** $h = 2$ to Total iterations **do**
 - 8: **for** $y_i \in V_y$, set $G_{y_i|1:p}^{(*)} = G_{y_i|1:p}^{(h-1)}$ **do**
 - 9: Randomly draw $z_k \sim V_z$
 - 10: Add/remove link from z_k to y_i : $G_{y_i, z_k|1:p}^{(*)} = 1 - G_{y_i, z_k|1:p}^{(h-1)}$
 - 11: Compute $\phi = \exp[\log P(Y|G_{y_i|1:p}^{(*)}) - \log P(Y|G_{y_i|1:p}^{(h-1)})]$. Draw $u \sim \mathcal{U}(0, 1)$.
 - 12: **if** $u < \min\{1, \phi\}$ **then** $G_{y_i|1:p}^{(h)} = G_{y_i|1:p}^{(*)}$ **else** $G_{y_i|1:p}^{(h)} = G_{y_i|1:p}^{(h-1)}$
-

Algorithm 2 Sampling $[G_0|Y, G_{1:p}, p]$

- 1: **Require:** Set of attributes $V_y = (y_1, \dots, y_n)$ and estimated lag network $G_{1:p}$
 - 2: Initialize $G_0^{(1)} = \emptyset$ and $G_{0:p}^{(1)} = [G_0^{(1)}, G_{1:p}]$
 - 3: **for** $y_i \in V_y$ **do**
 - 4: Set $V_{y_i} = V_y \setminus \{y_i\}$ and $\{z_\pi : G_{y_i, z_\pi|1:p} = 1\}$
 - 5: **for** $y_j \in V_{y_i}$ **do**
 - 6: Set $\pi_i = (y_j \cup z_\pi)$. Compute $\phi_a = P(Y|G_{y_i, z_\pi|0:p}^{(1)})$ and $\phi_b = P(Y|G_{y_i, \pi_i|0:p}^{(1)})$
 - 7: **if** $\phi_b > \phi_a$ **then** $G_{y_i, \pi_i|0:p}^{(1)} = 1$ **else** $G_{y_i, \pi_i|0:p}^{(1)} = 0$
 - 8: **for** $h = 2$ to Total iterations **do**
 - 9: **for** $y_i \in V_y$, set $G_{y_i|0:p}^{(*)} = G_{y_i|0:p}^{(h-1)}$ **do**
 - 10: Randomly draw $y_k \sim V_{y_i}$
 - 11: Add/remove link from y_k to y_i : $G_{y_i, y_k|0:p}^{(*)} = 1 - G_{y_i, y_k|0:p}^{(h-1)}$
 - 12: Compute $\phi = \exp[\log P(Y|G_{y_i|0:p}^{(*)}) - \log P(Y|G_{y_i|0:p}^{(h-1)})]$. Draw $u \sim \mathcal{U}(0, 1)$.
 - 13: **if** $u < \min\{1, \phi\}$ **then** $G_{y_i|0:p}^{(h)} = G_{y_i|0:p}^{(*)}$ **else** $G_{y_i|0:p}^{(h)} = G_{y_i|0:p}^{(h-1)}$
-

Appendix B. Network Statistics

In this section some useful network statistics are defined. See [Newman \(2010\)](#) for further material on network analysis.

Average Degree

Average degree is simply the average number of edges per node in the graph. It can be computed numerically as: Average Degree = Total Edges/Total Nodes.

Clustering Coefficient

Network clustering index is a measure of the tendency for nodes in a network form clusters or triangles. We apply the global clustering index of [Barrat and Weigt \(2000\)](#) which corresponds to the social network concept of transitivity and can be captured numerically as:

$$CC = \frac{3 \times (\text{number of triangles})}{(\text{number of open triads})}, \quad (\text{B.1})$$

where open triads are defined as a connected sub-graph consisting of three nodes and two edges. The index takes values between 0 and 1. It can be viewed as the probability of two neighbors of a node link to each other.

Average Path Length

The average path length is the average number of steps along the shortest paths for all possible pairs of network nodes. The average path length for a network with n -nodes is

$$APL = \frac{1}{n(n-1)} \sum_{i \neq j} SP_{ij}, \quad (\text{B.2})$$

where SP_{ij} is the shortest path between the nodes i and j .

Node Centrality

Node centrality in networks addresses the questions of how important a node/variable is in the network. Commonly discussed centrality measures include in-degree (number of in-bounds links), out-degree (number of out-bound links), authority, and hub scores. Let W be an n -node weighted graph without self-loop.

1. The authority score of node- i is a weighted sum of the power/hub score of the vertices with directed links towards node- i . They can be obtained via absolute value of the eigenvectors associated with the largest eigenvalue of (WW') . An authority node has a large in-degree.
2. The hub score of node- j is the weighted sum of the power/authority score of vertices with a directed link from node- j . They can be obtained via absolute value of the eigenvectors associated with the largest eigenvalue of $(W'W)$. A hub node usually has a large out-degree.

From a financial viewpoint, nodes with high authority scores/in-degree are highly influenced by others, while high hub scores/out-degree nodes are the influencers.

References

- Acharya, V.V., Pedersen, L.H., Philippon, T., Richardson, M., 2010. Measuring Systemic Risk. Working Paper 1002. Federal Reserve Bank of Cleveland.
- Adrian, T., Brunnermeier, M.K., 2016. CoVaR. American Economic Review 106 (7).
- Agudze, K.M., Billio, M., Casarin, R., Ravazzolo, F., 2021. Markov switching panel with network interaction effects. Journal of Econometrics, forthcoming.
- Ahelegbey, D.F., Billio, M., Casarin, R., 2016a. Bayesian Graphical Models for Structural Vector Autoregressive Processes. Journal of Applied Econometrics 31 (2), 357–386.
- Ahelegbey, D.F., Billio, M., Casarin, R., 2016b. Sparse Graphical Vector Autoregression: A Bayesian Approach. Annals of Economics and Statistics 123/124, 333–361.
- Ankargren, S., Jonéus, P., 2021. Simulation smoothing for nowcasting with large mixed-frequency VARs. Econometrics and Statistics 19, 97–113.
- Bai, J., 2000. Vector Autoregressive Models with Structural Changes in Regression Coefficients and in Variance-Covariance Matrices. Annals of Economics and Finance 1 (2), 303–339.
- Barigozzi, M., Brownlees, C., 2019. NETS: Network Estimation for Time Series. Journal of Applied Econometrics 34 (3), 347–364.
- Barnett, I., Onnela, J.-P., 2016. Change Point Detection in Correlation Networks. Scientific Reports 6, 18893.
- Barrat, A., Weigt, M., 2000. On The Properties of Small-World Network Models. The European Physical Journal B-Condensed Matter and Complex Systems 13 (3), 547–560.
- Berry, D., Hartigan, J.A., 1993. A Bayesian Analysis for Change Point Problems. Journal of American Statistical Association 88 (421), 309–319.
- Basu, S., Michailidis, G., 2015. Regularized Estimation in Sparse High-dimensional Time Series Models. The Annals of Statistics 43 (4), 1535–1567.
- Battiston, S., Delli Gatti, D., Gallegati, M., Greenwald, B., Stiglitz, J.E., 2012. Liaisons Dangereuses: Increasing Connectivity, Risk Sharing, and Systemic Risk. Journal of Economic Dynamics and Control 36 (8), 1121–1141.
- Bianchi, D., Billio, M., Casarin, R., Guidolin, M., 2019. Modeling Systemic Risk with Markov Switching Graphical SUR Models. Journal of Econometrics 210 (1), 58–74.

- Billio, M., Casarin, R., Rossini, L., 2019. Bayesian Nonparametric Sparse VAR Models. *Journal of Econometrics* 212 (1), 97–115.
- Billio, M., Getmansky, M., Lo, A.W., Pelizzon, L., 2012. Econometric Measures of Connectedness and Systemic Risk in the Finance and Insurance Sectors. *Journal of Financial Economics* 104 (3), 535–559.
- Casarini, R., Iacopini, M., Molina, G., ter Horst, E., Espinasa, R., Sucre, C., Rigobon, R., 2020. Multilayer network analysis of oil linkages. *The Econometrics Journal* 23 (2), 269–296.
- Chib, S., 1998. Estimation and Comparison of Multiple Change-point Models. *Journal of Econometrics* 86 (2), 221–241.
- Cho, H., Fryzlewicz, P., 2015. Multiple Change-point Detection for High-dimensional Time Series via Sparsified Binary Segmentation. *Journal of the Royal Statistical Society: Series B (Statistical Methodology)* 77 (2), 475–507.
- Commission, F.C.I., 2011. The Financial Crisis Inquiry Report: The Final Report of the National Commission on the Causes of the Financial and Economic Crisis in the United States. Public Affairs.
- Corander, J., Villani, M., 2006. A Bayesian Approach to Modelling Graphical Vector Autoregressions. *Journal of Time Series Analysis* 27(1), 141–156.
- Covitz, D., Liang, N., Suarez, G.A., 2013. The Evolution of a Financial Crisis: Collapse of the Asset-Backed Commercial Paper Market. *The Journal of Finance* 68 (3), 815–848.
- DasGupta, B., Kaligounder, L., 2014. On Global Stability of Financial Networks. *Journal of Complex Networks* 2 (3), 313–354.
- Diebold, F., Yilmaz, K., 2014. On the Network Topology of Variance Decompositions: Measuring the Connectedness of Financial Firms. *Journal of Econometrics* 182 (1), 119–134.
- Eichler, M., 2013. Causal inference with multiple time series: principles and problems. *Philosophical Transactions of the Royal Society A* 371 (1997).
- Erdman, C., Emerson, J.W., 2008. A Fast Bayesian Change Point Analysis for the Segmentation of Microarray Data. *Bioinformatics* 24 (19), 2143–2148.
- Fearnhead, P., 2006. Exact and Efficient Bayesian Inference for Multiple Changepoint Problems. *Statistics and Computing* 16 (2), 203–213.
- Fearnhead, P., Liu, Z., 2007. On-line Inference for Multiple Changepoint Problems. *Journal of the Royal Statistical Society: Series B (Statistical Methodology)* 69 (4), 589–605.
- Forbes, K.J., Rigobon, R., 2002. No Contagion, Only Interdependence: Measuring Stock Market Comovements. *The Journal of Finance* 57 (5), 2223–2261.
- Geiger, D., Heckerman, D., 2002. Parameter Priors for Directed Acyclic Graphical Models and the Characterization of Several Probability Distributions. *Annals of Statistics* 30 (5), 1412–1440.
- Green, P.J., 1995. Reversible Jump Markov Chain Monte Carlo Computation and Bayesian Model Determination. *Biometrika* 82 (4), 711–732.
- Gruber, L.F., West, M., 2017. Bayesian Forecasting and Scalable Multivariate Volatility Analysis Using Simultaneous Graphical Dynamic Models. *Econometrics and Statistics* 3, 3–22.
- Grzegorczyk, M., Husmeier, D., Rahnenführer, J., 2011. Modelling Non-stationary Dynamic Gene Regulatory Processes with the BGM Model. *Computational Statistics* 26 (2), 199–218.
- Hautsch, N., Schaumburg, J., Schienle, M., 2015. Financial Network Systemic Risk Contributions. *Review of Finance* 19 (2), 685–738.
- Hauzenberger, N., 2021. Flexible mixture priors for large time-varying parameter models. *Econometrics and Statistics* 20, 87–108.
- Hu, L., Guindani, M., Fortin, N.J., Ombao, H., 2020. A hierarchical Bayesian model for differential connectivity in multi-trial brain signals. *Econometrics and Statistics* 15, 117–135.
- IMF (2008). World Economic Outlook Update: Rapidly Weakening Prospects Call For New Policy Stimulus.
- IMF (2009). World Economic Outlook Update: Contractionary Forces Receding But Weak Recovery Ahead.
- Jochmann, M., Koop, G., Strachan, R.W., 2010. Bayesian Forecasting using Stochastic Search Variable Selection in a VAR Subject to Breaks. *International Journal of Forecasting* 26 (2), 326–347.
- Koop, G., Korobilis, D., Pettenuzzo, D., 2019. Bayesian Compressed Vector Autoregressions. *Journal of Econometrics* 210 (1), 135–154.
- Koop, G., Potter, S.M., 2007. Estimation and Forecasting in Models with Multiple Breaks. *The Review of Economic Studies* 74 (3), 763–789.
- Koop, G., Potter, S.M., 2009. Prior Elicitation in Multiple Change-Point Models. *International Economic Review* 50 (3), 751–772.
- Lèbre, S., Becq, J., Devaux, F., Stumpf, M.P.H., Lelandais, G., 2010. Statistical Inference of the Time-varying Structure of Gene Regulation Networks. *BMC Systems Biology* 4 (1), 130.
- Massacci, D., 2017. Least squares estimation of large dimensional threshold factor models. *Journal of Econometrics* 197 (1), 101–129.
- Massacci, D., 2021. Testing for regime changes in portfolios with a large number of assets: A robust approach to factor heteroskedasticity. *Journal of Financial Econometrics*, forthcoming.
- Newman, M., 2010. Networks: An Introduction. Oxford University Press.
- Nobile, A., Fearnside, A.T., 2007. Bayesian Finite Mixtures with an Unknown Number of Components: The Allocation Sampler. *Statistics and Computing* 17 (2), 147–162.
- Organization, W. H. (2003). Update 95-SARS: Chronology of a Serial Killer.
- Paci, L., Consonni, G., 2020. Structural Learning of Contemporaneous Dependencies in Graphical VAR Models. *Computational Statistics & Data Analysis* 144, 106880.
- Pesaran, M.H., Pettenuzzo, D., Timmermann, A., 2006. Forecasting Time Series Subject to Multiple Structural Breaks. *The Review of Economic Studies* 73 (4), 1057–1084.
- Qu, Z., Perron, P., 2007. Estimating and Testing Structural Changes in Multivariate Regressions. *Econometrica* 75 (2), 459–502.
- Ruggieri, E., 2013. A Bayesian Approach to Detecting Change Points in Climatic Records. *International Journal of Climatology* 33 (2), 520–528.
- Ruggieri, E., Antonellis, M., 2016. An Exact Approach to Bayesian Sequential Change Point Detection. *Computational Statistics and Data Analysis* 97, 71–86.
- Skripnikov, A., Michailidis, G., 2019. Joint estimation of multiple network Granger causal models. *Econometrics and Statistics* 10, 120–133.
- Western, B., Kleykamp, M., 2004. A Bayesian Change Point Model for Historical Time Series Analysis. *Political Analysis* 12, 354–374.
- Xuan, X., Murphy, K., 2007. Modeling Changing Dependency Structure in Multivariate Time Series. In: Proceedings of the 24th international conference on machine learning. ACM, pp. 1055–1062.